A Sensorized Hybrid Gripper to Evaluate a Grasping Quality Based on a Largest Minimum Wrench

Wookeun Park, Seongmin Seo, Jinhyeok Oh, and Joonbum Bae, *Member, IEEE*

***Abstract*—Soft pneumatic grippers, which are based on soft pneumatic actuators have been widely studied owing to their simple morphological structure, inherent compliance, and pliable grasp. Additionally, the integration of the soft gripper with various sensors to improve its functionality has also been extensively studied. Although the soft gripper is known to exhibit a robust grasping performance without accurate control, the grasping quality of the soft gripper has rarely been studied due to the lack of adequate embedded sensors and quality metrics of the soft gripper. Therefore, a hybrid gripper, which is a soft gripper with rigid components, was sensorized by embedding a soft force sensor and a bending sensor to evaluate the grasping quality. Furthermore, a new grasping quality metric for a soft gripper was proposed, which calculates the largest minimum wrench of a convex hull in the wrench space. The proposed grasping quality metric was experimentally verified, and a real-time program was developed to evaluate the grasping quality.**

***Index Terms*—Soft sensors and actuators, grasping, soft robot applications.**

I. Introduction

RECENTLY, soft pneumatic grippers (SPGs), which offer a more compliant bending motion than rigid robots owing to their simple morphological structure and higher degree of freedom, have been actively developed [1]–[3]. Moreover, to enhance their grasping performance such as actuation speed and finger force, soft pneumatic actuators (SPAs) have been developed in many ways [1]–[5]. Different chamber shapes, such as the fast pneumatic network (PneuNet), have been investigated for improved actuation speed [6]. Additionally, SPAs have also been reinforced by fiber, fabric, and integration with rigid and soft materials to realize enhanced fingertip forces [1]–[5].

Furthermore, various sensors have been embedded in the SPGs to increase their functionality [7]–[9]. Shih *et al.* integrated a soft sensor with the SPGs based on conductive-polydimethylsiloxane (cPDMS) for the haptic recognition of grasped objects [7]. Zhao *et al.* also developed a soft sensor based on optical waveguides for integration with a soft robotic hand to sense the different shapes and roughnesses of the grasped surfaces [9]. Chen *et al.* embedded a commercial bending sensor in the soft gripper to recognize the sizes of different objects [10]. However, the evaluation of the grasping quality how the gripper grasps the object well or not, may have not been studied.

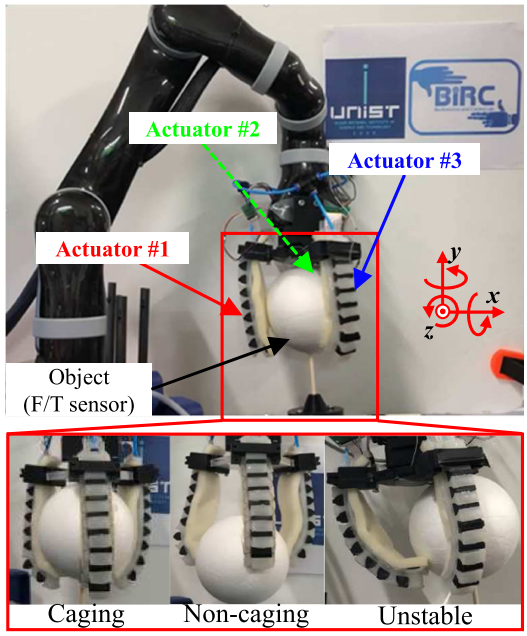

Fig. 1. Configuration of the sensorized hybrid gripper with the embedded soft force and bending sensors to evaluate the grasping quality depending on the difference postures (caging, non-caging, and unstable grasp).

Grasp synthesis based on measuring the quality metric has been developed for grasp planning [11]–[16]. Lei and Zheng *et al.* developed a grasp planning method to compare the force closure grasp based on the wrench space by computing every possible contact points [12]–[14]. Although Krug *et al.* evaluated the grasping quality using a rigid robotic gripper, which integrates with a tactile sensor array [17], it cannot be applied to a soft gripper due to the lack of adequate soft tactile sensors. Additionally, deep learning algorithms have also been developed for soft grippers. Choi *et al.* integrated a depth camera sensor with a soft gripper to predict the successful grasp using the learning technique. However, it may not be practically used because it requires an additional learning procedure. Thus, previous works

Manuscript received September 10, 2019; accepted January 26, 2020. Date of publication February 26, 2020; date of current version March 7, 2020. This letter was recommended for publication by Associate Editor C.-H. Yeow and Editor K.-J. Cho upon evaluation of the reviewers' comments. This work was supported in part by the National Research Foundation of Korea (NRF) Grant funded by the Korean Government (MSIT) NRF-2019R1A2C2084677 and NRF-2016R1A5A1938472, and in part by the 2020 Research Fund (1.200050.01) of UNIST (Ulsan National Institute of Science and Technology), and Institute for Information & communications Technology Promotion (IITP) Grant funded by the Korea government (MSIP) 2017000910001100, Development of multi-material 3D printing technologies for flexible motion detection and control sensor modules. *(Corresponding author: Joonbum Bae.)*

The authors are with the Bio-Robotics and Control (BiRC) Laboratory, Department of Mechanical Engineering, UNIST, Ulsan 44919, Korea (e-mail: wkpark@unist.ac.kr; tjtjdals2004@unist.ac.kr; jhoh@unist.ac.kr; jbbae@unist.ac.kr).

Digital Object Identifier 10.1109/LRA.2020.2976312

may not be used practically as a real-time application, since they may have limitations, such as 1) the adequate soft sensor is not developed for the grasping quality, and 2) the synthesis and learning techniques may be computationally expensive.

Thus, in this study, we developed a sensorized hybrid gripper, which can evaluate the grasping quality based on how it can resist external forces with different grasping postures, as depicted in Fig. 1. The hybrid gripper [5], which was previously developed for improved grasping abilities such as actuation speed and fingertip force or torque, was sensorized by embedding a soft force sensors and a bending sensor. The grasping quality was calculated by the force closure, which indicates how well the grasp can resist the external force or torque before it fails to grasp [18], [19]. Embedding sensors and calculating contact wrenches of the grasp were only introduced in a previous work [20], and the detailed analysis and experiments for grasping quality based on the largest minimum wrench (LMW) were covered in this paper. The main contributions of this study are as follows: 1) a sensorized hybrid gripper was developed by embedding a soft force sensor and a bending sensor in the hybrid gripper, 2) a new grasping quality metric for a soft gripper based on the LMW method, which evaluates the convex hull in the wrench space, was proposed, and 3) the proposed grasping quality was experimentally verified with different grasping postures, and the real-time program was developed to evaluate the grasping quality.

The remainder of this paper is organized as follows. In Sections II and III, brief introductions of the LMW method and sensorized hybrid gripper are provided, respectively. The calibration of the embedded sensors is discussed in Section IV. Experimental verification and a real-time application for the evaluation of the grasping quality using the sensorized hybrid gripper are discussed in Section V. Finally, the conclusion and future work are presented in Section VI.

II. Methodology for Grasping Quality

A. Grasping Quality Metric

The grasping quality metric is generally evaluated based on the geometries of the grasping posture and the contact forces. Considering the finger force of the gripper is limited, a sum of the resultant force by the contact force was suggested as the basic quality metric of the grasped object (Q_{SRF}) [21]. However, Q_{SRF} does not imply how well the grasp can resist in terms of the force equilibrium. The grasping posture based on the wrench, which indicates the force and torque applied to the grasped object, should be evaluated how well the grasp resist to external wrenches in the wrench equilibrium. Thus, the LMW-based quality metric (Q_{LMW}) [22], which evaluate the amount of external wrenches that the grasp can resist while the wrench equilibrium is, was suggested to overcome the limitation of Q_{SRF}.

B. Largest Minimum Wrench (LMW) Method

How large external force or torque, applied to the grasped object, is expressed by the wrench equilibrium as follows [22]:

$$\sum_{i=1}^{n} \omega_i + \omega_{ext} = 0 \tag{1}$$

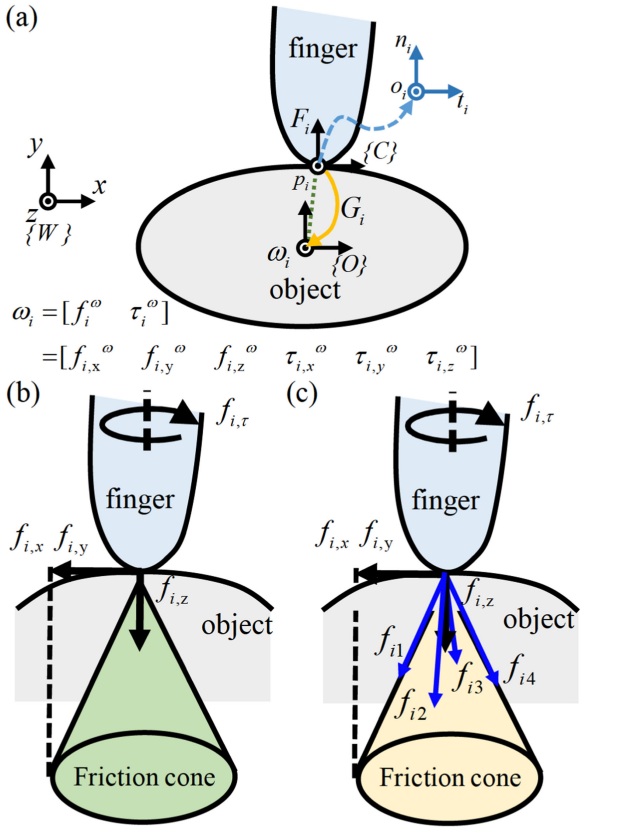

Fig. 2. Examples of the grasp map and contact force matrix : (a) grasp map in 3D object, (b) the soft contact model and (c) the reorganized soft contact model.

where i is the number of wrench. ω_i is the number of contact wrenches, and ω_{ext} indicates the external wrench that the grasp can resist. The grasping quality of a posture is determined by calculating the amount of external forces or torque that the contact wrenches. The wrench is calculated using the contact force matrix and grasp map as follows:

$$\begin{aligned} \omega_i &= G_i f_i \\ &= \begin{bmatrix} f_i^{\omega} & \tau_i^{\omega} \end{bmatrix}^T \\ &= \begin{bmatrix} f_i^{\omega} & \rho\tau_i^{\omega} \end{bmatrix}^T \end{aligned} \tag{2}$$

where i is the number of contact point, G_i and f_i represent the grasp map and the contact force matrix, respectively, and f_i and τ_i denote the force and torque element of the wrench (ω_i), respectively. To unify the units of the wrench, a scaling factor (ρ) was multiplied with the torque [12].

The grasp map G_i converts the coordinate from the contact point to the object to express the contact force into the wrench elements as depicted in Fig. 2(a). The grasp map is expressed as follows [19]:

$$G_i = \begin{bmatrix} o_i & t_i & n_i & 0 \\ p_i \times o_i & p_i \times t_i & p_i \times n_i & n_i \end{bmatrix} \tag{3}$$

where i is the number of contact point. p_i denotes the position of the contact point, and t_i, o_i, and n_i are the unit vectors in the

tangential and normal direction at the contact point in the object coordinate frame, respectively, as shown in Fig. 2(a).

The spatial force at the contact point was modeled as a soft contact (SC) model, as shown in Fig. 2(b), wherein the elastomeric material was used for the gripper [11]. The SC model, which is expressed as the friction cone, includes not only the normal force, but also the tangential forces, and the torsional force in the x, y, and z axes, expressed as follows:

$$\begin{aligned} f_i &= \begin{bmatrix} f_{i,x} & f_{i,y} & f_{i,z} & f_{i,\tau} \end{bmatrix} \\ &= \left\{ f_i | f_{i,z} \geq 0, \sqrt{\frac{f_{i,x}^2 + f_{i,y}^2}{\mu_i^2} + \frac{f_{i,\tau}^2}{\mu_{i,\tau}^2}} \leq f_{i,z} \right\} \end{aligned} \tag{4}$$

where i is the number of contact points on the gripper, and $f_{i,z}$ is the normal force at the contact position. $f_{i,x}$, $f_{i,y}$, and μ_i are the tangential forces and the friction coefficient, respectively. $f_{i,\tau}$ and $\mu_{i,\tau}$ are the torsional force and the torsional friction coefficient, respectively.

The SC model was reorganized for the computational convenience as the quadrangular pyramid [11], as depicted in Fig. 2(c). In the reorganized SC model, the contact force is divided into four elements (blue arrows in Fig. 2(c)), expressed as follows:

$$\begin{aligned} f_{ij} &= \left\{ f_{ij} | f_{ij} \in F_i, F_i = \sum_{j=1}^{n} \alpha_{ij} f_{ij} \right\} \\ &= \begin{bmatrix} \mu_i f_{ij,z} & \mu_i f_{ij,z} & f_{ij,z} & \mu_{i,\tau} f_{ij,z} \end{bmatrix} \end{aligned} \tag{5}$$

where i is the number of contact points and j denotes the number of divided force elements. n, and α_{ij} was determined as 4, and $1/4$, respectively, due to the pyramidal shape of the reorganized SC model (Fig. 2(c)). Thus, the contact force is expressed as f_{ij}, determined by $f_{ij,z}$, which is measured by the embedded sensors.

Finally, the convex hull of the wrench elements (ω_{CH}) is expressed as follows:

$$\omega_{CH} = \left\{ conv\left(\sum_{i=1}^{n} \omega_{ij} = \alpha_{ij} G_i f_{ij} \right) \middle| \alpha_{ij} f_{ij} \in F_i \right\} \tag{6}$$

where i is the number of contact and j is the divided force elements in the reorganized SC model. f_{ij} is the contact force matrix based on the reorganized SC model. The convex hull indicates the wrench applied to the grasped object and the magnitude of the external force or torque that can be resisted. The convex hull of the wrench space is evaluated using the radius of the largest ball, which is formed at the origin inside ω_{CH}. The minimum ball inside the convex hull wrench space is calculated using the minimum length of the distance from the origin to the plane of the convex hull space. The LMW-based quality metric (Q_{LMW}) is expressed as follows:

$$Q_{LMW} = \min_i (d_{CH,i}) \tag{7}$$

where i is the number of convex hull planes at each calculation, and $d_{CH,i}$ is the distance between the origin and the ith convex hull plane, respectively.

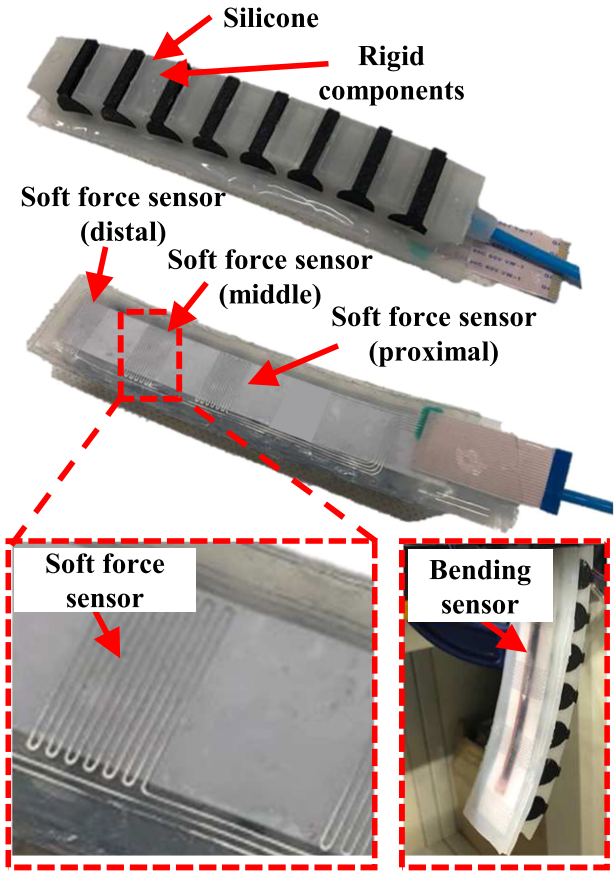

Fig. 3. Design of the sensorized hybrid PneuNet with the commercial bending sensor and customized soft force sensor.

III. Sensorized Hybrid Gripper

A. Introduction to Hybrid Gripper

The hybrid gripper, which is assembled using the hybrid PneuNet, was developed as in the previous work, and the fingertip force and the actuation speed was enhanced by the hybrid structures with soft and rigid materials, which induce the actuator moves in a circular motion without a twisting. The soft chamber, made of silicone (Dragonskin 30 A, Smooth-on [23]), was fabricated by 3D printed molds, and the rigid structure was manufactured by using a 3D printer (ABS-P430, Stratasys [24]). For the detailed design of the hybrid gripper, refer [5].

B. Embedding Sensors for Hybrid Gripper

A soft sensor based on eutectic-gallium indium (eGaIn), which was fabricated using the direct ink writing method [25], was embedded to measure the contact force, as illustrated in Fig. 3. The customized soft force sensor, which includes the microchannel filled with eGaIn, measures the changed resistance depending on the deformation of the microchannel. The readily-available bending sensor (Flex sensor 4.5," Spectrasymbol [26]), which also measures the changed resistance, was embedded for measuring the bending angle, as depicted in Fig. 3. The sensor

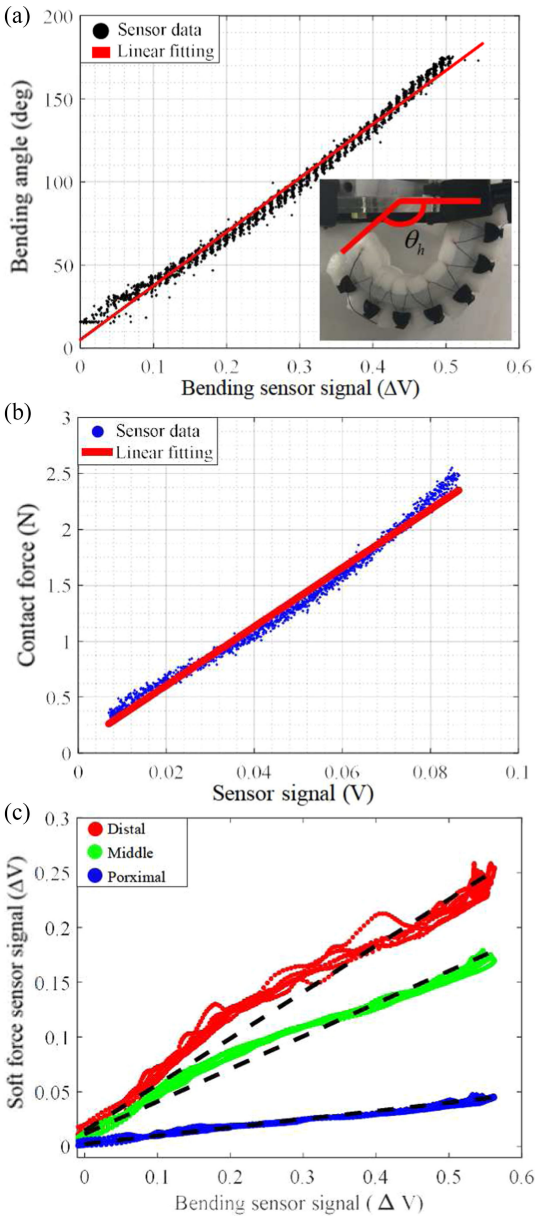

Fig. 4. Calibration for the embedded sensors: (a) relationship between the bending angle and the bending sensor, (b) relationship between the soft force sensor (distal point) and the contact force, (c) unwanted soft force sensor signals during the pure bending motion.

data were acquired via a simple voltage divider and amplifying circuit. The soft sensor was also attached to the palm of gripper to identify the contact of the object and the palm while the gripper grasp the object.

IV. Calibration of Embedded Sensors

A. Decoupling of Embedded Sensors

The bending angle (θ_h), measured by the bending sensor, was calibrated by the motion capture data, as depicted in Fig. 4(a). The soft force sensor was calibrated by the force/torque (F/T) sensor (ATI Gamma, ATI [27]). The sensorized hybrid PneuNet

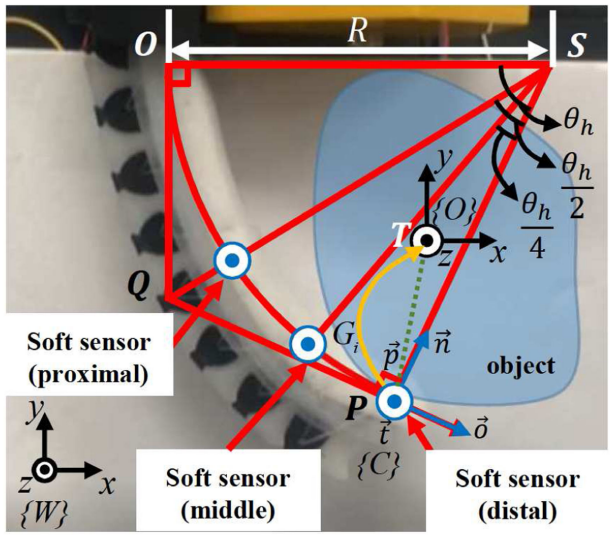

Fig. 5. Calculation of the the grasp map.

was fixed on the mount and the F/T sensor measured the contact force on the soft sensor at the distal point under 60 kPa. The normal force at the contact point ($f_{ij,z}$) was obtained by the linear relationship between the F/T sensor and soft force sensor data, as shown in Fig. 4(b). The same calibration was applied for the middle and proximal point owing to their similar microchannel shape of the soft sensor.

The resistance of the microchannel for the customized soft force sensor is changed due to the elongation of the layer, which contains the soft sensor, while the hybrid PneuNet was bent by the inflation. Therefore, to reduce the unwanted soft sensor signals, the soft force sensor data was subtracted by the offset ($V_{i,cal}$), which was calculated by the bending sensor data. $V_{i,cal}$ is expressed as follows :

$$V_{i,cal} = V_{i,org} - (\alpha_i V_{bend} + \beta_i) \tag{8}$$

where i is the number of customized soft sensor. $V_{i,org}$ is the original soft force sensor signal before decoupling. $V_{i,cal}$ is the decoupled soft force sensor signal by using the bending sensor signal (V_{bend}) during the free bending motion. α_i and β_i are parameters, obtained by the linear fitting, as depicted in Fig. 4(c).

B. Calculation of Grasp Map and Contact Force Matrix

The grasp map at the contact points, including the proximal, middle, and distal points converts the contact force to the contact wrench in terms of the object coordinate, as illustrated in Fig. 5. It was assumed that the gripper moves in a pure circular trajectory without twisting motion owing to the hybrid structure with a soft and rigid materials, and the triangular palm design. The tip position of the gripper was also assumed that it is not dragged due to the weight of the grasped object. The grasp map at the distal point in a world frame ($\{W\}$) was expressed using the

bending angle θ_h as follows:

$$
\begin{aligned}
R &= \frac{L_0}{\theta_h} \\
\overrightarrow{OP} &= (R - R\cos\theta_h, -R\cos\theta_h, 0) \\
\overrightarrow{OS} &= (R, 0, 0) \\
\overrightarrow{OQ} &= \left(0, -R\tan\left(\frac{\theta_h}{2}\right) 0, 0\right)
\end{aligned}
\tag{9}
$$

where R, and L_0 are the radius of the curvature and initial length, as depicted in Fig. 5. An analytically modeled p_i was calculated using $\overrightarrow{OP}$ and $\overrightarrow{OT}$, which is determined by the origin of the hybrid PneuNet (O), attached to the palm, as illustrated in Fig. 5. n_i and o_i were also obtained by the normalized $\overrightarrow{PS}$ and $\overrightarrow{QP}$, respectively, calculated by the $\overrightarrow{OP}$, $\overrightarrow{OS}$, and $\overrightarrow{OQ}$. Lastly, t_i was calculated by a cross product of o_i and n_i. Because the soft force sensors for the middle and proximal points are located at the $1/4$, and $1/2$ point of L_0, the grasp map at the middle and proximal points was determined by the $\theta_h/4$ and $\theta_h/2$, respectively, instead of θ_h. The grasp map of the other finger was obtained by multiplying the rotation matrix in the y axis considering the triangular palm shape.

The contact force matrix was obtained by the customized soft sensor (4), which measure the normal force element ($f_{i,z}$). The friction coefficient and torsional friction coefficient between the rigid and rubber material, which are set to 4.0 and 0.3 considering the radius of gyration (75 mm) for the sensorized hybrid gripper, respectively [28]. The contact force matrix at each contact point was obtained by the soft force sensor.

V. Experiments for Grasping Quality Based on LMW

When calculating Q_{LMW}, the scaling factor ρ, which indicates the maximum moment arm for the possible contact points, was applied for the torque wrench elements to unify the units, as expressed in (2). Considering the maximum radius of the grasped spherical object, which is determined by the triangular palm shape, ρ was set to 60 mm. The quality metric was classified into $Q_{LMW,force}$ and $Q_{LMW,torque}$ to express the grasping quality in terms of the force and torque independently. $Q_{LMW,force}$ and $Q_{LMW,torque}$ were obtained by the convex hull calculation via only the force, and torque elements, respectively. The convex hull of the wrench space was calculated through the MATLAB library [29].

The grasping quality was calculated when the pressure was applied for the sensorized hybrid gripper, whereas the sensor data were acquired via a data acquisition device (NI PCIe-6353, National Instruments [30]). We demonstrated the different postures for the spherical dummy object to evaluate the grasping qualities in 4 s of inflation, as depicted in Fig. 1. The caging posture represents a grasp with all fingers including palm contact, and the non-caging posture represents a grasp with only the distal points of fingers. The unstable grasp refers to the grasping of an object wherein at least one finger is not involved in the grasp. In the case of the caging grasp, the reaction force from the palm was

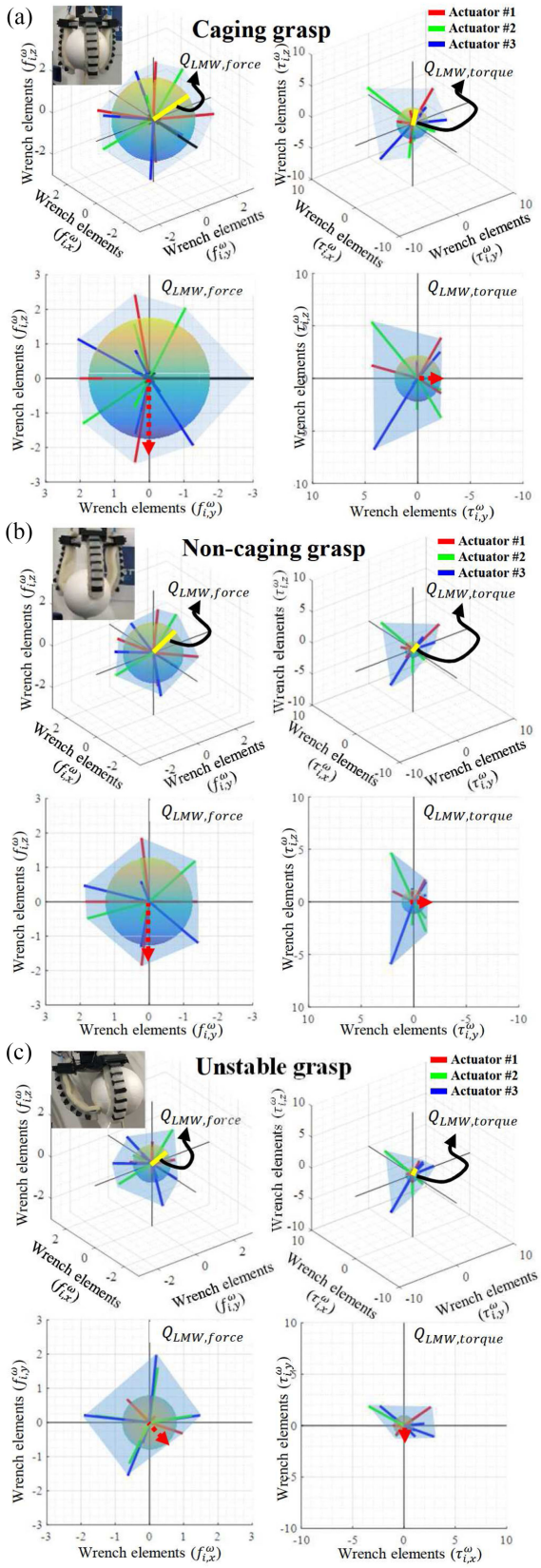

Fig. 6. Wrench elements and grasping quality calculation: (a) force and torque elements in three dimensional (3-D) space, and projected on yz plane for the caging grasp, (b) force and torque elements in 3-D space, and projected on yz plane for the non-caging grasp, (c) force and torque elements in 3-D space, and projected on xy plane for the unstable grasp.

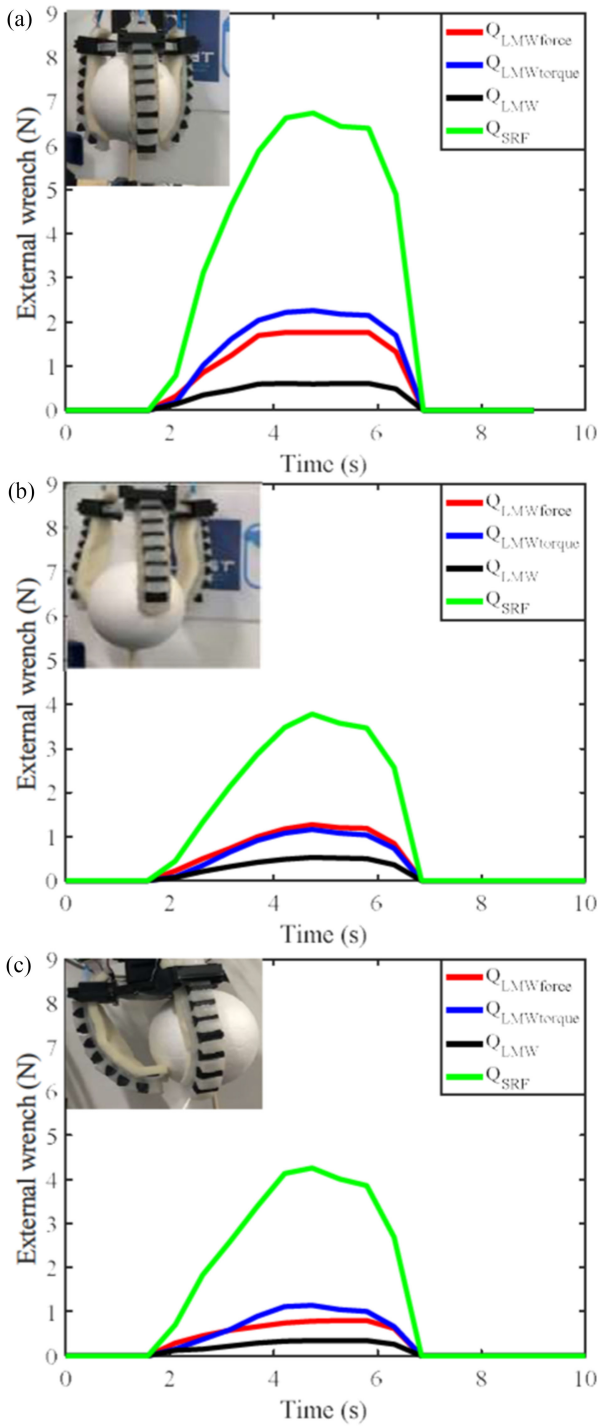

Fig. 7. Evaluated grasping qualities based on different grasping postures: (a) caging grasp, (b) non-caging grasp, (c) unstable grasp.

added to determine the convex hull wrench space (ω_{CH}). The caging and non-caging grasps were determined by the contact at the palm that the additional soft sensor was attached to sense the contact.

A. Calculation of Grasping Quality

The convex hull wrench spaces of the force and torque elements for each grasping posture are plotted in Fig. 6. The blue transparent area indicates the convex hull space, as illustrated in Fig. 6. The radius of the ball at the origin, depicted in Fig. 6, indicates how the grasp can resist the external force and torque in any direction. The radii, illustrated as yellow lines in Fig. 6, imply the evaluation of convex hull wrench space (ω_{CH}) for the force, and torque elements ($Q_{LMW,force}$, and $Q_{LMW,torque}$). The wrench elements of the different grasping posture, resulted in the difference in ω_{CH}, differentiate the grasping quality. For example, $Q_{LMW,force}$ and $Q_{LMW,torque}$ of the caging grasp were evaluated to be larger than those of the non-caging grasp, as the wrench elements were more inclined to the y axis, and the contact wrench at the palm was added for forming ω_{CH}, as illustrated in Fig. 6(a) and (b). As the unstable grasp showed small grasping quality based on LMW due to the absence of contact wrench of the actuator#1 for the grasp (Fig. 6(c)), the grasping quality of unstable grasp is smaller than those of the caging and non-caging grasp.

TABLE I
GRASPING QUALITY EVALUATION FOR THE DIFFERENT GRASPING POSTURES (Unit : N)

	$Q_{LMW,force}$	$Q_{LMW,torque}$	Q_{LMW}	Q_{SRF}
Caging	1.76	2.22	0.60	6.39
Non-caging	1.27	1.16	0.52	3.78
Unstable	0.80	1.01	0.34	4.13

As the ball at the origin, illustrated in Fig. 6, indicates how it can maximally resist in any external wrenches, the weak direction of the external wrench can also be analyzed. To specify the weak direction, the convex hull wrench space was projected onto a two dimensional plane as depicted in Fig. 6. The weak direction was depicted as red-dashed arrows, shown in Fig. 6, considering how much the external wrench is needed to disturb the wrench equilibrium (1). For the caging grasp and non-caging grasp, the directions of the external force and torque are in the z direction and y direction, respectively (red-dashed arrows in Fig. 6(a), and (b)). In the case of the unstable grasp, as the wrench elements by actuator#1 were less than those of the other grasps, the weak direction of the external force and torque were in $(x, y, z) = (1/\sqrt{2}, -1/\sqrt{2}, 0)$, and the y direction, respectively, depicted as red-dashed arrows in Fig. 6(c).

The LMW-based quality metrics (Q_{LMW}, $Q_{LMW,force}$, and $Q_{LMW,torque}$), and simple quality metric based on the resultant force (Q_{SRF}) of the caging, non-caging, and unstable grasps are illustrated in Fig. 7. The maximum quality metrics during the grasping are presented in Table I. The caging and non-caging grasp are distinguished more clearly by comparing not only Q_{LMW} but also $Q_{LMW,force}$ and $Q_{LMW,torque}$. The caging and non-caging grasps have less quality metric differences in terms of Q_{LMW} and $Q_{LMW,force}$, as depicted in Fig. 7(a), and (b). However, when the grasping quality of those grasps are compared by $Q_{LMW,torque}$, it is more clear than evaluating with other quality metric, since the caging posture grasp the object in a caging shape.

The non-caging and unstable grasp may be evaluated more clearly by comparing Q_{LMW}, $Q_{LMW,force}$, and $Q_{LMW,torque}$, rather than Q_{SRF}. Even if the unstable grasp has a larger Q_{SRF} than that of the non-caging grasp, the non-caging grasp has a

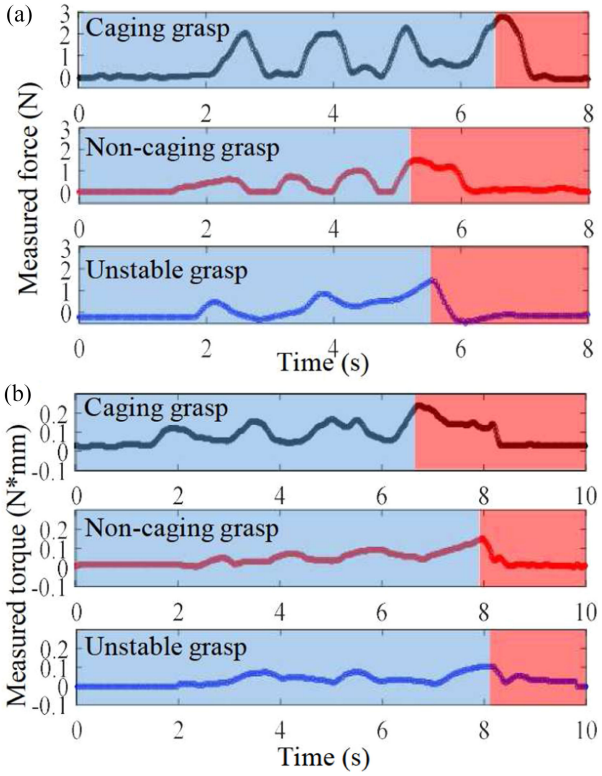

Fig. 8. Experimental verification in terms of external wrenches in weak direction for (a) $Q_{LMW,force}$ of caging, non-caging, and unstable grasp, (b) $Q_{LMW,torque}$ of caging, non-caging, and unstable grasp. The blue, and red-shaded area indicates the grasping success, and failure, respectively.

larger Q_{LMW} than that of the unstable grasp, which implies the non-caging grasp can resist the external wrenches, as depicted in Fig. 7(b), and (c). It may be important to evaluate the grasping quality of different grasps of soft gripper to utilize the quality metrics based on LMW method including Q_{LMW}, $Q_{LMW,force}$, and $Q_{LMW,torque}$ rather than simple sum of resultant forces, Q_{SRF}.

B. Experimental Verification of Grasping Quality

The evaluated grasping qualities of the caging, non-caging, and unstable grasps were experimentally verified using the F/T sensor. The dummy object, mounted on the F/T sensor, was grasped under different grasping postures and pulled three or four times in the weak direction, which was analyzed in the previous section. The blue and red-shaded areas, illustrated in Fig. 8(a) and (b), indicate the grasping postures that can resist or fail to grasp the object from the external wrench. For the comparison of $Q_{LMW,torque}$ and reference torque from F/T sensor, ρ was also multiplied to reference torque. The caging grasp failed to grasp the object until 1.9 N of x directional force, and 2.37 N (0.2 N·m) of y directional torque. The non-caging grasp failed to grasp the object at 1.2 N of z directional force, and 1.68 N (0.14 N·m) of y directional torque. Lastly, the unstable grasp missed the object at 1 N of $(x, y, z) = (1/\sqrt{2}, -1/\sqrt{2}, 0)$ directional force or 1.04 N (0.09 N·m) of y directional torque. Thus, the maximum resisting external wrenches for each grasp in the spatial force and torque are similar to those of the evaluated grasping quality.

TABLE II
GRASPING QUALITY DEPENDING ON d (Unit : N)

	$Q_{LMW,force}$	$Q_{LMW,torque}$	Q_{LMW}	Grasp
sphere (d=0 mm)	1.23	2.37	0.43	Y
sphere (d=20 mm)	0.86	1.68	0.36	Y
sphere (d=40 mm)	0.61	1.04	0.18	N
cubic (d=0 mm)	1.42	1.66	0.54	Y
cubic (d=20 mm)	0.74	1.47	0.31	Y
cubic (d=40 mm)	0.58	1.33	0.22	N
doll (d=0 mm)	1.20	2.40	0.40	Y
doll (d=20 mm)	0.74	1.47	0.37	Y
doll (d=40 mm)	0.66	1.11	0.12	N

C. Real-Time Application

Successful and unsuccessful grasps for the test objects were determined by whether all the quality metrics satisfied the threshold or not as a real-time application [30], depicted in Fig. 9. Considering the feasible grasping volume of the gripper, which is decided by the gripper design, the different objects including the unstructured (doll), spherical, and cubical objects, which are hardly deformed during grasp, were selected. The grasping quality of test objects were evaluated depending on the different x directional distance (d) between the center of the palm and the object, as shown in Fig. 9(a) and Table II. As the test objects have similar size and shape, which induce the similar grasping posture and contact forces of the gripper, the grasping quality metrics for each object in the same grasping condition were calculated as same as shown in Table II. Thus, the same threshold was applied for grasping the test objects in the real-time application.

Considering the external torque or force, the grasping quality metrics, evaluated by the developed sensorized hybrid gripper, can also be applied for the feedback control of robotic manipulation. The user interface, which includes the embedded sensor data, and the grasping quality is depicted in Fig. 9(b). The blue and red-dashed box indicates the success or failure of the grasp for the doll, and please refer the supplementary video clip for the application of the dummy objects.

VI. CONCLUSION

The hybrid gripper, which was previously developed to enhance the fingertip force and actuation speed, was sensorized to improve its functionality. Additionally, it was used to evaluate the grasping quality using the commercial bending sensor and customized soft force sensors to measure the grasping posture and contact forces. The grasping quality based on the wrench space, which indicates how the grasp can resist the external force in all the directions (Q_{LMW}). Q_{LMW} was divided into detailed

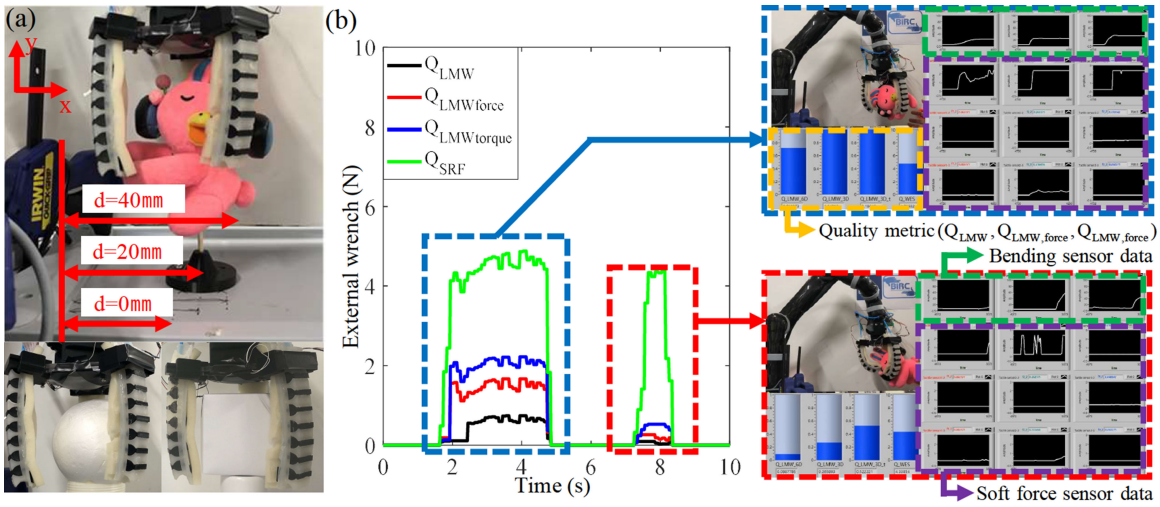

Fig. 9. Real-time application: (a) experiment for determining the threshold of grasping quality (doll, spherical, and cubical objects), (b) real-time grasping quality evaluation program applied for the doll grasping.

two quality metrics ($Q_{LMW,force}$ and $Q_{LMW,torque}$) to evaluate the different grasping postures. The grasping quality for the spherical object was evaluated and experimentally verified using the F/T sensor. The measured grasping quality metric was also applied for the real-time application of diagnosing the grasping success for the robotic grasping manipulation.

For future work, since the grasping quality was evaluated for the similar-sized object due to the grasping volume of the gripper, the comprehensive experiments for evaluating the grasping quality of the objects with different size and shape will be conducted. In addition, to reduce the error of analytical model for the grasp map, we aim to determine the grasping posture using the learning algorithm with the embedded sensors.

REFERENCES

[1] J. Zhou, S. Chen, and Z. Wang, "A soft-robotic gripper with enhanced object adaptation and grasping reliability," *IEEE Robot. Autom. Lett.*, vol. 2, no. 4, pp. 2287–2293, Oct. 2017.

[2] K. C. Galloway *et al.*, "Soft robotic grippers for biological sampling on deep reefs," *Soft Robot.*, vol. 3, no. 1, pp. 23–33, 2016.

[3] P. Polygerinos *et al.*, "Modeling of soft fiber-reinforced bending actuators," *IEEE Trans. Robot.*, vol. 31, no. 3, pp. 778–789, Jun. 2015.

[4] Y. Chen, F. Wan, T. Wu, and C. Song, "Soft-rigid interaction mechanism towards a lobster-inspired hybrid actuator," *J. Micromechanics Microengineering*, vol. 28, no. 1, 2017, Art. no. 014007.

[5] W. Park, S. Seo, and J. Bae, "A hybrid gripper with soft material and rigid structures," *IEEE Robot. Autom. Lett.*, vol. 4, no. 1, pp. 65–72, Jan. 2018.

[6] B. Mosadegh *et al.*, "Pneumatic networks for soft robotics that actuate rapidly," *Adv. Functional Mater.*, vol. 24, no. 15, pp. 2163–2170, 2014.

[7] B. Shih *et al.*, "Custom soft robotic gripper sensor skins for haptic object visualization," in *Proc. Intell. Robots Syst., IEEE/RSJ Int. Conf.*, 2017, pp. 494–501.

[8] G. Gerboni, A. Diodato, G. Ciuti, M. Cianchetti, and A. Menciassi, "Feedback control of soft robot actuators via commercial flex bend sensors," *IEEE/ASME Trans. Mechatronics*, vol. 22, no. 4, pp. 1881–1888, Aug. 2017.

[9] H. Zhao, K. OBrien, S. Li, and R. F. Shepherd, "Optoelectronically innervated soft prosthetic hand via stretchable optical waveguides," *Sci. Robot.*, vol. 1, no. 1, 2016, Art. no. eaai7529.

[10] Y. Chen, S. Guo, C. Li, H. Yang, and L. Hao, "Size recognition and adaptive grasping using an integration of actuating and sensing soft pneumatic gripper," *Robot. Auton. Syst.*, vol. 104, pp. 14–24, 2018.

[11] M. A. Roa and R. Suárez, "Computation of independent contact regions for grasping 3-d objects," *IEEE Trans. Robot.*, vol. 25, no. 4, pp. 839–850, Aug. 2009.

[12] Y. Zheng, "An efficient algorithm for a grasp quality measure," *IEEE Trans. Robot.*, vol. 29, no. 2, pp. 579–585, 2012.

[13] Z. Yu, "Computing the best grasp in a discrete point set with wrench-oriented grasp quality measures," *Auton. Robots*, vol. 43, no. 4, pp. 1041–1062, 2019.

[14] Q. Lei and M. Wisse, "Object grasping by combining caging and force closure," in *Proc. 14th Int. Conf. Control, Autom., Robot. Vision*, 2016, pp. 1–8.

[15] X. Zhu and J. Wang, "Synthesis of force-closure grasps on 3-d objects based on the q distance," *IEEE Trans. Robot. Autom.*, vol. 19, no. 4, pp. 669–679, Aug. 2003.

[16] C. Choi, W. Schwarting, J. DelPreto, and D. Rus, "Learning object grasping for soft robot hands," *IEEE Robot. Autom. Lett.*, vol. 3, no. 3, pp. 2370–2377, Jul. 2018.

[17] R. Krug, A. J. Lilienthal, D. Kragic, and Y. Bekiroglu, "Analytic grasp success prediction with tactile feedback," in *Proc. IEEE Int. Conf. Robot. Autom.*, 2016, pp. 165–171.

[18] M. A. Roa and R. Suárez, "Grasp quality measures: Review and performance," *Auton. Robots*, vol. 38, no. 1, pp. 65–88, 2015.

[19] B. León, A. Morales, and J. Sancho-Bru, *From Robot to Human Grasping Simulation*. Berlin, Germany: Springer, 2014.

[20] W. Park, S. Seo, and J. Bae, "Development of a sensorized hybrid gripper to evaluate grasping quality," in *Proc. 2nd IEEE Int. Conf. Soft Robot.*, 2019, pp. 149–154.

[21] B. Mirtich and J. Canny, "Easily computable optimum grasps in 2-d and 3-d," in *Proc. IEEE Int. Conf. Robot. Autom.*, 1994, pp. 739–747.

[22] M. A. Roa and R. Suárez, "Grasp quality measures: review and performance," *Auton. Robots*, vol. 38, no. 1, pp. 65–88, 2015.

[23] Smooth-On, "Smooth-On Dragonskin 30," 1895. [Online]. Available: https://www.smooth-on.com

[24] STRATASYS, "STRATASYS uPrinter SE PLUS," 1989. [Online]. Available: http://www.stratasys.com

[25] S. Kim, J. Oh, D. Jeong, W. Park, and J. Bae, "Consistent and reproducible direct ink writing of eutectic gallium–indium for high-quality soft sensors," *Soft Robot.*, vol. 5, no. 5, pp. 601–612, 2018.

[26] Spectrasymbol, "FS-L-0095-103-ST," 2018. [Online]. Available: spectrasymbol.com

[27] ATI industrial automation, "ATI nano 17 force/torque sensor," 1989. [Online]. Available: http://www.ati-ia.com

[28] E. Oberg and F. D. Jones, *Machinery's Handbook*. New York, NY, USA: Industrial Press, 1916, vol. 1916.

[29] Mathworks, "MATLAB," 1984. [Online]. Available: https://www.mathworks.com/products/matlab.html

[30] National Instruments, "NI," 1984. [Online]. Available: https://www.ni.com/ko-kr.html